


Article

Extended Development of a Fission Gas Release Behavior Model Inside Spherical Fuel Grains for LWR Reactors

Jingyu Guo ¹, Songbai Cheng ^{1,2}, Kai Wang ^{1,*} and Wenzhong Zhou ^{1,*}

¹ Sino-French Institute of Nuclear Engineering and Technology, Sun Yat-Sen University, Zhuhai 519082, China; guojy65@mail2.sysu.edu.cn (J.G.); chengsb3@mail.sysu.edu.cn (S.C.)

² College of Nuclear Science and Technology, Harbin Engineering University, Harbin 150001, China

* Correspondence: wangk326@mail.sysu.edu.cn (K.W.); zhouwzh3@mail.sysu.edu.cn (W.Z.)

Abstract: Fission gas plays a significant role in fuel rod performance following accidents. The amount of fission gas increases dramatically under accidental conditions. This leads to a subsequent rise in the fuel rod internal pressure and temperature due to aggravated gap conductance between the fuel pellet and cladding. As a result, fuel rod performance degrades. Therefore, studying fission gas behavior is crucial for accident assessment and evaluating fuel rod performance. Minimizing the impact of fission gas on fuel rods is essential for maintaining their integrity and safety within nuclear reactors. One important aspect of ensuring safety is predicting fission gas release (FGR). In this study, we presented an extended model to be used in light water reactors (LWRs). The FGR can be modeled using COMSOL Multiphysics with the finite element method. This modeling approach considers both normal and abnormal conditions, with the latter categorized as Class-II type incidents. The model assumes that the gas diffusion inside a spherical grain varies over time. By examining perfect sinks with gas production, perfect sinks without gas production, and imperfect sinks under steady-state conditions, different initial and boundary conditions are set. To validate the accuracy and universality of expressions used in the model, input parameters from other models and experiments are utilized. By comparing the model's results with these inputs, the accuracy and applicability of the expressions can be confirmed. This validation process ensures that the model provides reliable predictions for fission gas behavior in fuel rods under both normal and abnormal operating conditions. Based on our findings, it is evident that the FGR fraction displays an upward trend as diffusion coefficients and temperatures rise. Conversely, larger grain sizes and higher linear heat generation rates are associated with a reduction in the FGR fraction. Notably, enhanced resolution leads to a postponed onset of FGR. Furthermore, the influence of the diffusion coefficient on the FGR fraction primarily stems from the interconnected effects of temperature and linear heat generation rate.

Keywords: fission gas release (FGR); fission gas diffusion; fission gas behavior; light water reactor; accidental condition



Citation: Guo, J.; Cheng, S.; Wang, K.; Zhou, W. Extended Development of a Fission Gas Release Behavior Model Inside Spherical Fuel Grains for LWR Reactors. *Appl. Sci.* **2023**, *13*, 10421. <https://doi.org/10.3390/app131810421>

Academic Editors: Jeong Ik Lee and José A. Orosa

Received: 15 June 2023

Revised: 23 August 2023

Accepted: 30 August 2023

Published: 18 September 2023



Copyright: © 2023 by the authors. Licensee MDPI, Basel, Switzerland. This article is an open access article distributed under the terms and conditions of the Creative Commons Attribution (CC BY) license (<https://creativecommons.org/licenses/by/4.0/>).

1. Introduction

The operation of the fuel elements in a nuclear reactor core is essential to the safety of the nuclear reactor. Ensuring the safety and integrity of nuclear fuels is of the utmost importance for their development in both normal and emergency situations [1]. Early research reactors have been utilized to investigate theories and conduct experiments on fission gas behavior [2]. The variation in grain size has no effect on the release threshold in the LWR. The grain size can only affect the release rate when the grain boundary is networked [3]. Fission gas will enter the gap between the fuel and cladding in the LWR when the fuel fails in the high enthalpy condition of reactivity-initiated accidents (RIAs) [4]. The intragranular swelling rate is subjected to fission gas in the PWR fuel rod [5]. The FGR sharply elevates with increasing temperature at the initial phase and then tends towards moderation in the PWR during irradiation. FGR occurs via diffusion of gas atoms at the

opening grain boundary [6]. The FGR is subjected to gas sweeping on the grain boundary in the PHWR [7]. The simulation results show that fission products raise with grain diameter in the VVER [8].

After the Fukushima accident, the international community recognized the need for advanced fuel designs that offer substantially improved performance under severe accidents, leading to the U.S. Department of Energy's Nuclear Energy Office (DOE-NE) launching the Accident Tolerant Fuel Campaign (ATF Campaign). The safety margin of nuclear power plants (NPPs) can be enhanced by improving the oxidation-resistant performance of fuel cladding. There are primarily three types of advanced fuel cladding. The first is Cr-coated Zr-based cladding, which possesses several merits. It can improve the peak cladding temperature limit during the design of basic LOCA and extend the time of before post-quench ductility failure occurs [9]. Meanwhile, Chromium coated on ATF is viewed as one of the most promising forms of ATF cladding. In terms of its resistance to high-temperature oxidation and deformation, the retention of fission products, and heat transfer between the coolant and cladding, the performance of ATF cladding is better than conventional Zr-based cladding [10]. The second type of advanced fuel cladding is FeCrAl alloys that can resist oxidation under high temperature and steam conditions. And the last type of cladding is Si/SiC cladding, which is the best among the three cladding materials in terms of its oxidation resistance and high-temperature strength; therefore, it has been called the ideal ATF cladding material [9]. Innovative fuel systems must be implemented to enhance fuel, plant work, and safety to meet or exceed design benchmark accidental conditions [11]. While current reactor designs predict the behavior of fission gases within fuel rods over their operational lifetime, current fuel designs are not able to compensate for over-lifetime gas release, and an extended burnup extent in existing reactors is a significant issue [12].

The behavior of gaseous fission products under irradiation conditions heavily impacts nuclear fuel rod performance [13]. The released fission gases access the rod's free space, which increases the internal pressure of the rod or creates bubbles, leading in fuel swelling and enhanced pellet cladding mechanical interactions (PCMIs). The above processes affect the mechanical behavior of rods [14], while the FGR reduces the thermal conductivity between the fuel and cladding. Gases within bubbles degrade the thermal conductivity of the fuel, ultimately influencing the temperature distribution of the fuel pellets. As a result [15], fission gases significantly affect the thermal properties of fuel rods. When fission gases enter bubbles, the fuel swells and mechanically interacts with the fuel cladding, closing the gap between the fuel and cladding. Fission gas release (FGR) causes the pressure in the rod free space to increase as well as causing the thermal conductivity of the rod filling gas to degrade.

The safety of nuclear reactors and ultimate fuel repositories are assessed by utilizing nuclear fuel performance codes, with prediction for FGR being a crucial aspect. In fuel performance codes, FGR typically includes two steps [14]. First, based on the linear power rating, fission gas atoms are generated through fission reactions, and some of the gas atoms move to the grain boundaries via diffusion, with thermal diffusion during high temperatures being the primary form. In addition to thermally activated defects, irradiation-enhanced defect concentrations drive gas atoms to diffuse, with athermal diffusion under low temperatures being important. The released gas atoms are particularly relevant to the thermal conductivity of fuels with fast neutron factors, like nitride fuels, for which the release fraction at high temperatures may be lower than oxide fuels; however, the thermal conductance of the gap also deteriorates. Second, the concentration and release threshold of gas atoms causes the gas atoms to release and be stored on the grain boundaries. This behavior is affected by temperature and other properties.

When analyzing the thermal-mechanical performance of fuel rods, fission gas behavior is a significant aspect, and this behavior is modeled by fuel performance codes. Modeling this behavior in nuclear fuels under irradiation involves accounting for various interactive phenomena. Gas atoms are produced inside fuel grains and diffuse towards grain bound-

aries. Bubbles precipitating and growing at the grain faces leads to fuel swelling. After bubble growth and interlink, the gas atoms release from the grain faces, causing thermal FGR. Gas atoms and the vacancy diffusion of bubbles contribute to the development of this process. Except for these diffusion ways, experiments have also justified that micro-cracking is mechanism of grain face separation, and gas atoms may be released from grain boundaries through these cracks, resulting in significant FGR in transient situations. These fast kinetics typically take a burst release into account. Under irradiation experiments, the FGR rate raises due to cracking on the grain boundaries, which is caused by fission gas accumulating and inducing thermal stresses. After transient heating, grain surfaces exhibit the phenomenon of planar separation, and the stored gas atoms release through the cracking along a particular area between two grains. Micro-cracking occurs at grain face causing grains unable to store gas atoms and thus leadin to additional fission gas release during transient situations [14].

According to Tonks et al. 2018, [16], fuel performance is affected by the amount and release of fission gases in UO_2 fuel, causing the fuel to swell and the gap pressure to increase. The majority of FGR undergoes three processes: first, gases are generated and move from bulk; second, bubbles in the grain face nucleate, grow, and interlink until they adhere to grain boundaries; third, gas atoms are transported through interlinkage grain boundary passages until they arrive at a free surface and are released. Gas atom diffusion primarily determines the above mechanisms, although knockout, recoil, and burst release may cause some gas atoms to release.

As mentioned earlier, nuclear fuel performance is greatly affected by fission gas behavior. Moreover, fission gas behavior is related to the integrity and safety of nuclear power plants [17].

Indeed, the behavior of fission gases is of utmost importance in understanding and managing nuclear reactors, particularly in the context of nuclear accidents such as Chernobyl and Fukushima. In the case of Chernobyl, the accident was caused by a combination of design flaws, operator errors, and a rapid power excursion that led to a destructive steam explosion and a subsequent graphite fire. The release of fission products, including fission gases such as xenon and krypton, played a significant role in the dispersion of radioactive material into the atmosphere. Similarly, the Fukushima accident was triggered by a massive earthquake and tsunami that resulted in the loss of power and cooling capabilities at the Fukushima Daiichi nuclear power plant. The subsequent overheating and melting of fuel assemblies led to the release of fission gases and other radioactive materials into the environment. Studying the behavior of fission gases under severe accident conditions helps in assessing the consequences and developing strategies for mitigating their release and dispersal. Research on fission gas behavior encompasses various aspects, including gas release mechanisms, diffusion and transport within fuel materials, retention in fuel rods, and the potential effects on fuel performance and reactor safety. By gaining a deeper understanding of these factors, scientists and engineers can develop improved fuel designs, safety systems, and accident management strategies to enhance the overall safety and reliability of nuclear reactors.

It is worth noting that significant advancements have been made in the field of fission gas behavior research over the years, contributing to the development of more robust and accident-tolerant fuel designs, improved reactor operation and maintenance practices, and enhanced safety measures in the nuclear industry. However, fission gas behaviour is very complicated, as it includes FGR, fission gas diffusion, grain growth, and swelling. On the other hand, different types of nuclear fuels may behave differently. It is relatively easy to simulate single fission gas behavior, such as FGR processes under steady state conditions, but this fails to reflect the thermal fission gas behaviour in the nuclear reactor. A more sophisticated fission gas behaviour model is strongly needed to better understand this phenomenon.

UO_2 fuels have been successfully and broadly used as primary fuels in commercial light water reactors. The prediction of fission gas behaviour is important for fuel rod

performance when a reactor operates at stable conditions. The fission gas is released when the gas reaches a saturation value in the grain boundaries. The fuel rod pressure and temperature continue to increase with gas release due to the degradation of gap thermal conductance between the pellet and cladding. In this study, we considered both FGR and diffusion for the gas behavior. We mainly focused on investigating the parameter sensitivity of FGR in LWR through simulations. The effect of grain growth was implicitly considered by using FGR with different grain sizes. COMSOL Multiphysics was used for the modeling of UO_2 grain geometry and for solutions to relevant equations. The FGR over time, the fission gas diffusion coefficient, and burnup with temperature under three different conditions in a light water reactor (LWR) are discussed in this study. The FGR with unequal grain sizes, diffusion coefficients, temperatures and linear heat generation rates with different working conditions are compared.

2. Methods

The extended model is based on previous theories and empirical formulations [18–26]. The thermomechanical properties and their relevant equations are given in reference [15].

The mechanism of FGR includes two components: athermal and thermal FGR [27]. Athermal release happens at a high burnup when gas atoms escape from the free surfaces of the fuel through recoil and knockout. When the temperature exceeds the incubation threshold, thermal release drops with increasing temperature [28]. The exact value of the threshold can be derived from the occurrence of intergranular gas. Gas atoms diffuse from the inner side of the fuel grains to the grain boundaries. The diffusion velocity rises with temperature.

In addition, a part of intergranular atoms is brought back into the solution through fission spikes. This is known as resolution. The resolution flux will prevent the flux diffusion to some extent. Resolution occurs within the grain, where atoms enter and form small bubbles. These bubbles eventually reintegrate into the solution through recombination and resolution, restoring equilibrium.

The mathematical framework of Booth [29] and Speight [24] provided a good solution method to the diffusion problem. Booth offered analytical expressions for constant irradiation under the LWR operating conditions, and two cases were used to present steady and transient state conditions in LWR that regarded the constant gas production case as the steady state condition and the zero-gas production case as the transient condition. Diffusion is neglected during transient operation since the power level is high enough for the gas production. The limitations of this study include the assumption of a perfect sink boundary condition, where there is a release as soon as gas atoms reach the grain boundary. In this case, the concentration at the grain boundary is zero in the mathematical expression. Resolution was later introduced by Speight to improve the Booth model [24]. Furthermore, the concentration at the grain boundary under imperfect sink conditions remains finite. Turnbull derived a closed form analytical solution for the model [25].

The extended model we present here is based on real physical process. The magnitude order of the physical quantities is important for matching the numerical algorithm to best suit the physical problem. In order to ensure the accuracy of a wide range of algorithm conditions, all the situations encountered in the normal and abnormal operations of the LWR were restricted to Class-II incidents.

The FGR model adopts an idealized spherical UO_2 grain. The parameters and expressions are given, such as the grain size and the diffusion coefficient of Xenon inside UO_2 . These parameters are essential to solve the ensuing mathematical problem efficiently. The details of the parameters are presented below.

2.1. Grain Size

The grain grows with increasing temperature, which introduces negative effects. However, to simplify the model, one can fix the grain size and ignore the effects of grain growth. This approach overlooks the impact of grain growth on the diffusion coefficient

and subsequently on gas release. When grain growth occurs, the diffusion coefficient tends to decrease, leading to reduced gas release. This relationship poses a complex problem that requires solving the diffusion equation with a moving boundary. The decreasing diffusion coefficient affects the rate at which gas is released due to grain growth. Additionally, grain growth results in the clustering of gas on the grain boundaries, which enhances gas release. This gas sweeping effect occurs as the grains grow, leading to increased gas release from the material. By comparing the computational results of fixed grain size without gas sweeping and grain growth with gas sweeping, it is evident that the latter exhibits higher gas release.

2.2. Diffusion Coefficient

In Turnbull et al. [30,31], the diffusion coefficient consists of the intrinsic diffusion in the absence of irradiation, and the thermal and athermal diffusion produced by irradiation can be derived. Owing to the irradiation-induced resolution of intragranular bubbles, the diffusion coefficient combined with Speight's theory is revised as follows [24]:

$$D = \frac{D_{1+2+3}}{1 + g/b'} \quad (1)$$

$$D_{1+2+3} = D_1 + D_2 + D_3 \quad (2)$$

$$g = D_{1+2+3}/L^2 \quad (3)$$

$$D = \frac{1}{1/(D_{1+2+3}) + 1/(L^2 b')} \quad (4)$$

$$D_1 = D_{01} \exp\left(\frac{-T_{01}}{T_K}\right) \quad (5)$$

$$D_2 = D_{02} \exp\left(\frac{-T_{02}}{T_K}\right) \sqrt{\frac{P'}{20}} \quad (6)$$

$$D_3 = D_{03} \frac{P'}{20} \quad (7)$$

Part of the parameters are accessed from reference [30–32], where D is diffusion coefficient; D_{1+2+3} is sum of the intrinsic, thermal, and athermal diffusion coefficients; g is probability of fission spikes trapping atoms within intragranular bubbles [27]; b' is probability of the resolution of these atoms by fission spikes; D_1 is intrinsic diffusion coefficient; D_2 is thermal diffusion coefficient; D_3 is athermal diffusion coefficient; L is mean free path between two bubbles; D_{01} , D_{02} , and D_{03} are diffusion constants; T_K is the local temperature; T_{01} and T_{02} are the parameters of the diffusion coefficient calculation; and P' is linear heat generation rate (LHGR). The parameters of these equations are given as: $D_{01} = 3.9 \times 10^{-6} \text{ m}^2/\text{s}$, $T_{01} = 45,275 \text{ K}$, $D_{02} = 1.77 \times 10^{-15} \text{ m}^2/\text{s}$, $T_{02} = 13,800 \text{ K}$, $D_{03} = 4 \times 10^{-21} \text{ m}^2/\text{s}$, $L^2 b' = 10^{-15} \text{ m}^2/\text{s}$.

Intrinsic diffusion represents the motion of clusters of gas atoms. Compared with low temperatures, the phenomenon of intrinsic diffusion is more easily observed at high temperatures. Gas atoms diffuse towards grain boundaries and accumulate on the grain boundaries. When the number of gas atoms saturates the grain boundaries and the temperature exceeds the incubation threshold, gas atoms begin to diffuse from the grain boundary towards the outside under the temperature gradient. This is the process of thermal diffusion. Athermal diffusion dominates at low temperatures. Recoil is the primary mechanism by which gas atoms move, resulting from collision between these atoms. This phenomenon leads to a slower saturation.

The above diffusion coefficients vary with temperature and are calculated and presented in Figure 1. This figure indicates that fission gas diffusion is affected by intrinsic diffusion, thermal diffusion, and athermal diffusion. In particular, intrinsic diffusion is one of the most influential items for the diffusion coefficient. Furthermore, the range of variation with temperature is the largest among all the diffusion coefficients. Without

considering the athermal fission gas release, the value of the athermal diffusion coefficient is constant. Figure 1 shows a summary of the previous models and experimental results. Comparing Figure 1a,b, the diffusion coefficient in our model is within a reasonable range compared with the other models and experimental results. In addition, the diffusion coefficient of different fuels is compared, such as UO₂, MOX, and UN. Although the results of UO₂ are greater than other fuels, there is a difference between its diffusion coefficient in the calculations and measurements due to different methods being used. For example, Combette and Zacharie used $D = 32,887 \times 10^{-53,527/T}$ to calculate the diffusion coefficient. Different temperature and burnup ranges were selected.

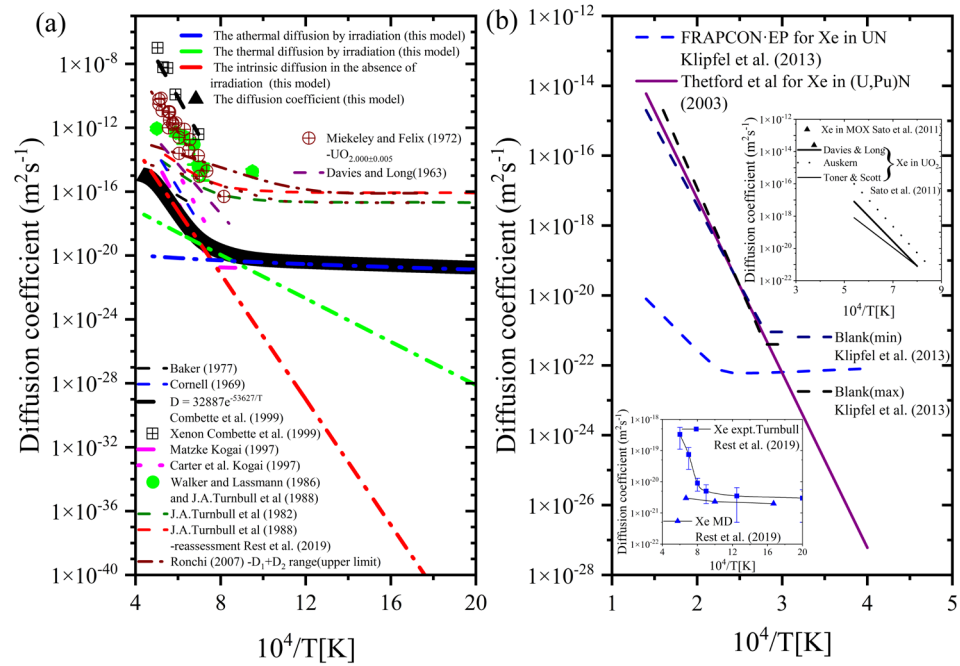


Figure 1. Variations in diffusion coefficients with temperature in models and experiments (a) (Combette and Zacharie, 1999; Guo et al., 2022; Kogai, 1997; Rest et al., 2019; Baker, 1977; Cornell, 1969; Davis and Long, 1963; Miekeley and Felix, 1972; Ronchi, 2007; Turnbull et al., 1982, 1989; Walker and Lassmann, 1986) [12,17,31,31,33–40] (b) (Guo et al., 2022; Klipfel et al., 2013; Rest et al., 2019; Sato et al., 2011, Thetford and Mignanelli, 2003) [12,17,41–43].

2.3. The Incubation Threshold

According to the previous theoretical and experimental results [18], some of the gas that remained inside the intergranular bubbles is brought back into solution through fission spikes. The equation for resolution flux is as follows:

$$J_{rs} = (bN)/2 \tag{8}$$

where J_{rs} is the resolution flux, b is the probability of the intergranular atoms re-entering the solution, and N is density per unit area at the grain boundaries. Here, we assume that the resolution flux is similar to the diffusion flux in Fick’s law. Then, the mean concentration at the grain boundaries is obtained:

$$c_{\delta} = (bN\delta)/(2D) \tag{9}$$

where c_{δ} is the mean concentration at the grain boundaries and δ is the resolution depth. The flux exit of the grain is as follows [24]:

$$J = J_0(1 - c_{\delta}/(\beta t)) \tag{10}$$

where J is flux exit of the grain, J_0 is flux without resolution, β is creation rate, and t is time. For a spherical grain of a defined radius, the flux is:

$$J_0 = \frac{1}{4\pi a^2} \frac{d}{dt} \left(\frac{4}{3} \pi a^3 \beta F_0 t \right) \tag{11}$$

where a is grain radius and F_0 is fission gas release fraction without resolution. The fission gas release fraction (%) without resolution approximately derives from the Booth diffusion model at a low release level:

$$F_0 = \frac{4}{\sqrt{\pi}} \frac{\sqrt{Dt}}{a} \tag{12}$$

The surface density at the grain boundaries ($1/m^2$) is as follows:

$$\frac{d}{dt} N = 4\beta \frac{\sqrt{Dt}}{\sqrt{\pi}} \left(1 - \frac{Nb\delta}{2Dt\beta} \right) \tag{13}$$

Based on the above equation, the surface density is time dependent. The incubation time is also related to the threshold value of the surface density. Its value is composed of two asymptotic solutions at low and high temperatures when the diffusion coefficient is constant over time:

$$T_{low} : t_i \sim (bN_s\delta) / (2D\beta) \tag{14}$$

$$T_{high} : t_i \sim \left(\frac{9}{8\pi} \right)^{1/3} \left(\frac{N_s}{\beta} \right)^{2/3} \frac{1}{D^{1/3}} \tag{15}$$

where T_{high} and T_{low} are the high and low temperatures for diffusion, respectively; t_i is incubation time; and N_s is the threshold value of the surface density. The incubation burnup is then taken as the incubation time:

$$T_{low} : Bu \sim \frac{bN_s\delta}{2(D_2 + D_3)} \tag{16}$$

$$T_{high} : Bu \sim \left(\frac{9}{8\pi} \right)^{1/3} (N_s)^{2/3} \beta^{1/3} \left(\frac{1}{D + L^2 b'} \right)^{1/3} \tag{17}$$

where Bu is the burnup. The above two asymptotic expressions can be integrated into a single expression due to the following two important remarks:

First,

$$T_{02} \sim T_{01} / 3 \tag{18}$$

Second, many parameters are uncertain, such as b , δ , and N_s . Thus, the solution form of the incubation threshold must be sought:

$$Bu = \frac{B_1}{\exp(-T_B/T_K) + B_2(T_K - B_3)} + B_{MIN} \tag{19}$$

where B_1 , B_2 , B_3 , and B_{MIN} are all adjustable parameters of the incubation threshold calculation in the model and T_B is the parameter of the incubation threshold calculation. Its values are taken from previous literature [44]. In this case, Parameters are given in this calculation: $B_1 = 1$ MWd/tM, $B_2 = 3.3 \times 10^{-8} \text{ K}^{-1}$, $B_3 = 603 \text{ K}$, $B_{MIN} = 1500$ MWd/tM, and $T_B = T_{02} = 13,800 \text{ K}$. The variation in the thermal threshold is presented in Figure 2. The burnup decreases with temperature. High temperatures correspond to a low burnup. The burnup of nuclear fuel increases within the reactor over time and is highest at the end of its operational life. The temperature drops with burnup. This corresponds to the reality of engineering. The variations in burnup at different temperatures represents the incubation threshold or thermal threshold, which is related to gas atoms diffusion. At low temperatures, athermal diffusion is dominant. At high temperatures, intrinsic and

thermal diffusion are more important than athermal diffusion for gas atoms. The results of the incubation threshold calculated using different equations in the Bernard model are extremely closed. The values of the threshold calculated using different equations in this model are slightly different, and there is a little difference between the Bernard model and this model. However, the threshold value calculated using Equation (19) is different. This difference may be the result of some uncertain fuel parameters. The threshold value calculated using Equation (13) in this model is comparable with the Bernard model.

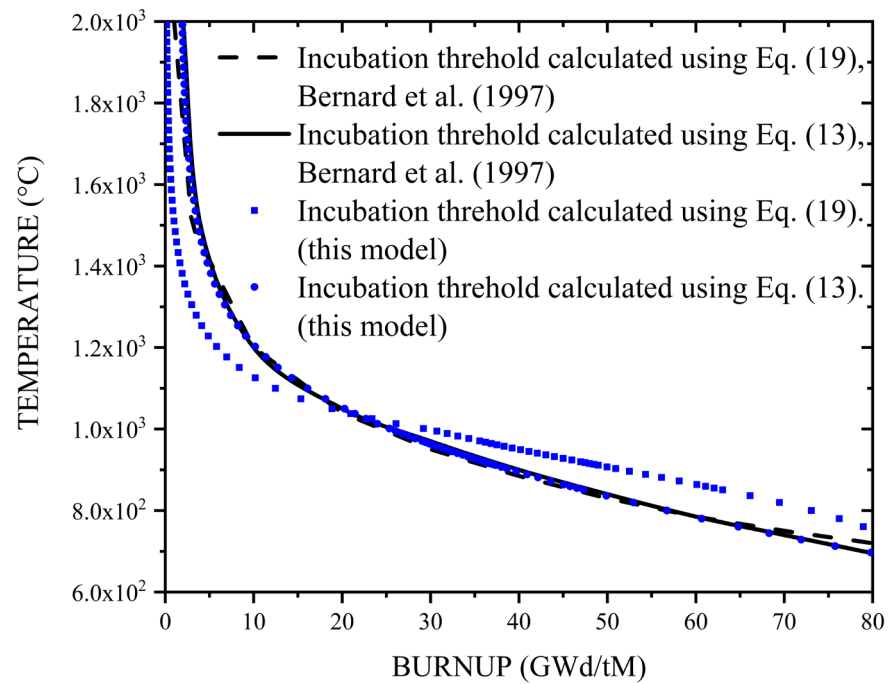


Figure 2. The incubation threshold in this model and the Bernard model [44].

The value of N_s is derived by assuming that the intergranular atoms accumulate in bubbles [26]. The calculated equations are as follows:

$$PV_B = nkT \tag{20}$$

$$n_B n = N_s \tag{21}$$

$$n_B = F_B / \pi R_B^2 \sin^2 \theta \tag{22}$$

$$P = P_{EXT} + 2\gamma / R_B \tag{23}$$

$$V_B = (4\pi/3) R_B^3 f(\theta) \tag{24}$$

$$f(\theta) = 1 - \frac{3}{2} \cos \theta + \frac{1}{2} \cos^3 \theta \tag{25}$$

by combining the above relations, we obtain:

$$N_s = [4f(\theta) / 3kT \sin^2 \theta] (P_{EXT} + 2\gamma / R_B) R_B F_B \tag{26}$$

where P is the bubble pressure, V_B is the bubble volume, n is number of atoms in a bubble, k is Boltzmann constant, T is the temperature, n_B is the bubble density, F_B is the fraction coverage of the bubbles, R_B is the bubble radius, θ is the semihedral angle, P_{EXT} is the pressure, γ is the free surface energy, and $f(\theta)$ is the geometry factor of the grain-edge bubble to the sphere. The exact values are given in the previous literature [44]:

$\gamma = 1 \text{ J/m}^2$, $R_B = 5 \times 10^{-7} \text{ m}$, $F_B = 0.25$, $\theta = 50^\circ$, and $f(\theta)/\sin 2\theta = 0.288$. The threshold value of the surface density varies from 10^{19} m^{-2} (like the value of a mono-atomic layer) to $3 \times 10^{20} \text{ m}^{-2}$ between the limiting two cases $P_{EXT} = 0 \text{ MPa}$ and $P_{EXT} \sim 120 \text{ MPa}$ (UO_2 fraction threshold) [45]. For instance, the value of P ($\sim 90 \text{ MPa}$) [46] corresponds to the threshold of the value of the surface density ($\sim 10^{20} \text{ m}^{-2}$) [47]. Equation (13) is presented in Figure 2 as the dashed curve, where $N_S = 3 \times 10^{20} \text{ m}^{-2}$, $T_K = 1273 \text{ K}$, and $b = 2 \times 10^{-6} \text{ s}^{-1}$. Figure 2 shows that some minor differences exist between the solid and the dashed curve, but the two lines approximately match.

The preceding parameter values will change when another gas equation of state is used in the ideal gas law. However, the order of magnitude of the threshold of value of the surface density does not change. For example, when a hard sphere equation of state is used, the value varies from $2 \times 10^{20} \text{ m}^{-2}$ to $3 \times 10^{20} \text{ m}^{-2}$ [48].

2.4. The Diffusion Equation

According to the kinetics of diffusion, fission gases diffuse from the inner side of the grain to the grain boundary. This mechanism is used in this model. The diffusion formulation is expressed as follows [44]:

$$\frac{\partial c}{\partial t} = \beta + \text{div}(D \text{grad}(c)) \quad (27)$$

where c is local concentration. The local concentration $c(r, t)$ is related to the space and time variable. The boundary condition is given by Equation (9).

3. Model Validation

To test the feasibility of our model, three standard cases were adopted.

3.1. Perfect Sink with Gas Production

In this case, the boundary conditions are $\beta = \text{constant}$, $c(r, 0) = 0$, and $c(a, t) = 0$ [44]. Namely, the concentration on the grain boundary is kept at zero and the diffusion formulation can be solved. The initial concentration of gas atoms both on the grain center and boundary is zero. When the gas atoms reach the grain boundaries, fission gas will release immediately. Gas atoms are generated constantly throughout this process. This case belongs to the LWR steady-state operation.

An analytical expression for the release fraction is given by Booth [29]:

$$F(t) = 1 - \frac{6a^2}{Dt} \left[\sum_{n=1}^{\infty} \frac{1 - \exp(-n^2\pi^2Dt/a^2)}{n^4\pi^4} \right] \quad (28)$$

where $F(t)$ is fission gas release fraction and $T = 900 \text{ }^\circ\text{C}$ and $P' = 20 \text{ kW/m}$ are typical LWR steady-state operational conditions. $D = 1.78 \times 10^{-20} \text{ m}^2/\text{s}$ and $a = 5 \times 10^{-6} \text{ m}$ is supposed. The corresponding burnup is approximately 70 GWd/tM under the irradiation. The analytical solution is presented in Figure 3. The result demonstrates that this case is comparable with the Bernard model.

3.2. Perfect Sink without Gas Production

In addition to the perfect sink condition, LWR Class-I and Class-II type conditions are adopted in this case. The boundary conditions are $\beta = 0$, $c(r, 0) = \text{constant} = c_0$, and $c(a, t) = 0$ [44]. No gas production was assumed. The initial concentration exists on the grain boundary, but the final concentration on the grain boundary is decreased to zero. Subsequently, the diffusion formulation is solved. The initial concentration of gas atoms is zero on the grain boundary and remains finite in the grain center. Once the gas atoms reach the grain boundaries, fission gas will release immediately. Gas atoms are not generated constantly during this process. This process is similar to the first case, but the onset of FGR

is faster than the first case owing to its initial gas atoms concentration on the grain center. The process is relevant to the LWR's transient operation.

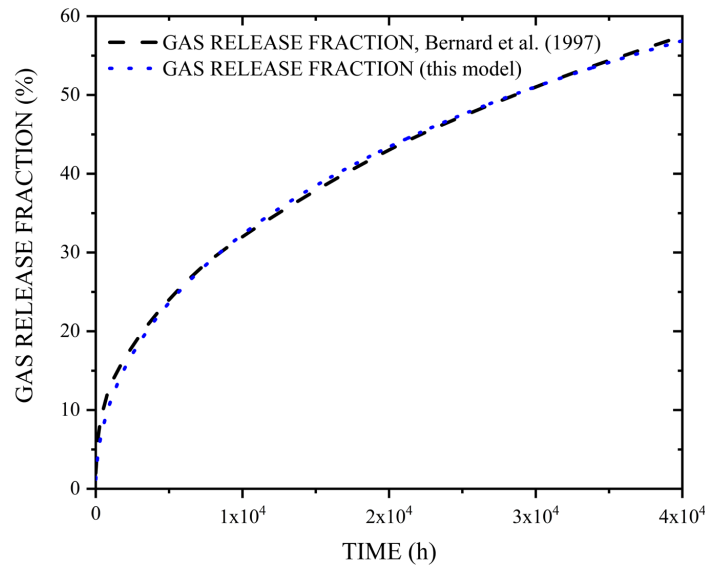


Figure 3. Gas release fraction versus time for constant gas production [44] (Bernard and Bonnaud, 1997).

The analytical solution is as follows [29]:

$$F(t) = 1 - 6 \sum_{n=1} \frac{\exp(-n^2\pi^2Dt/a^2)}{n^2\pi^2} \tag{29}$$

where c_0 is the initial concentration. In this case, $T = 1500 \text{ }^\circ\text{C}$, $P' = 40 \text{ kW/m}$, $D = 3.2 \times 10^{-17} \text{ m}^2/\text{s}$, and $t = 10 \text{ h}$. These parameters are typical of the upper-bound limit of all Class-I conditions. The parameters show that the linear heat generation rate is mildly higher than the perfect sink condition, but the time is much shorter than in the former case. For an upper-bound limit of all Class-II incidents, the condition will be more extreme. Meanwhile, the fission gas release fraction will decrease. The result is presented in Figure 4. This case compares well with the Bernard model.

3.3. Imperfect Sink

In this case, the diffusion formulation of the boundary condition is $\beta = \text{constant}$, $c(r, 0) = \text{constant} = c_0$, and $c(a, t) = c_\delta = (bN_S\delta)/(2D)$ [44]. This case is considered a resolution. The gas atoms reach the grain boundary and are not released quickly. Only when the concentration of the gas atoms reaches saturation concentration can the gas atoms release from the grain boundaries.

The analytical solution is as follows [25]:

$$F(t) = 1 - \frac{6}{\beta t} \sum_{n=1} \left(\frac{\beta a^2}{Dn^4\pi^4} - \frac{c_0 - c_\delta}{n^2\pi^2} \right) \left[1 - \exp(-n^2\pi^2Dt/a^2) \right] \tag{30}$$

The parameters are the same as in the perfect sink condition. Additional parameters are given as follows: $c_0 = 2.15 \times 10^{26} \text{ m}^{-3}$ and $c_\delta = 3.15 \times 10^{25} \text{ m}^{-3}$. The most significant difference from the other two cases is that the fission gas release begins at 20,000 h. The result shown in Figure 5 reflects that although there are some differences between this case and the Bernard model, the fraction of gas released in this case is higher than the Bernard model, and the range of relative error is limited to an acceptable range within 5%.

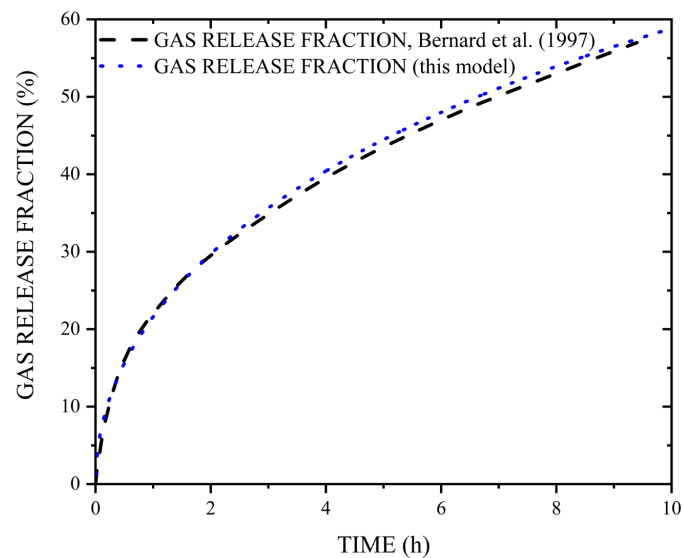


Figure 4. Gas release fraction versus time without gas production [44].

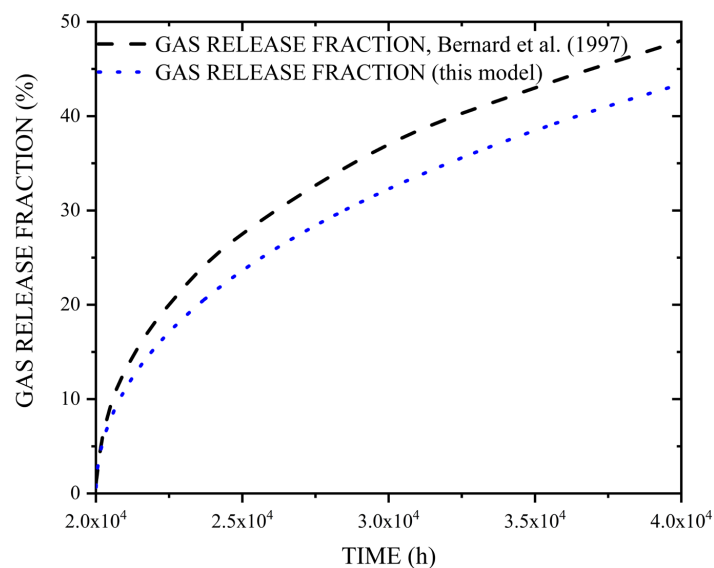


Figure 5. Gas release fraction versus time for constant gas production [44].

4. Model Application

By comparing the results of the above cases between this model and Bernard's model, we have shown that our model can predict well the above cases. In this section, the parameters of other models will be incorporated into this model. The validated scenarios in the model primarily consist of the aforementioned two cases. Then, the results will be compared and analyzed between this study and other models' processing to validate its effectiveness.

Fission gas release for uranium dioxide fuel was modeled using a new mechanistic and engineering approach [49]. The parameters $T = 1050$ °C, $P' = 18$ kW/m, $D = 5.8510 \times 10^{-20}$ m²/s, and $t = 3000$ h were selected, and the irradiation range was approximately 70 GWd/tU. This situation is close to the first case. Namely, the initial concentration of gas atoms both on the grain center and boundary are zero. The gas atoms are generated constantly and then diffuse towards the grain boundaries during LWR steady-state operation. The gas atoms begin to release when they reach the grain boundaries. The release of gas atoms lasts for 3000 h. There are three radiuses for fission gas release: 10 μm, 20 μm and 40 μm. Figure 6 shows that the results are similar in these

two models. Furthermore, this figure demonstrates that the FGR fraction decreases with increasing grain size.

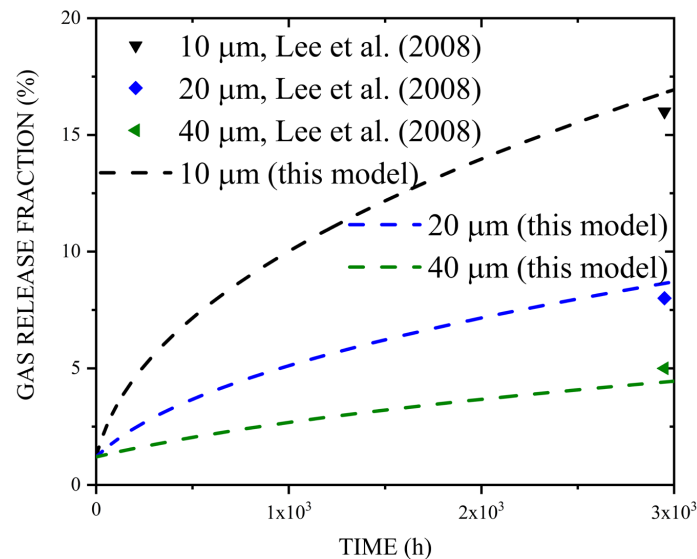


Figure 6. Gas release fraction versus time for constant gas production with different grain sizes in this model and Lee's model [49] (Lee et al., 2008).

Coupling with the FALCON code, fission gas release was modeled using uranium dioxide fuel [5]. The conditions were as follows: $T = 500$ °C, $P' = 20$ kW/m, $D = 4.0312 \times 10^{-21}$ m²/s, and $t = 40,000$ h, the irradiation range was approximately 75 GWd/tU. The first case is chosen here. The initial concentration of gas atoms both on the grain center and the boundary are zero. Gas atoms are generated constantly and then diffuse towards the grain boundaries during LWR steady-state operation. The gas atoms begin to release when they reach the grain boundaries. The release of gas atoms lasts 40,000 h. There are two radiuses for fission gas release: 9 μm and 51 μm. As shown in Figure 7, the results of this model and Khvostov's model are not fitted as well. This may be related to the fact that the FGR fraction is sensitive to the grain size.

Another case of the FGR was reported in oxide fuels for sodium fast reactors [50]. Its parameters were $T = 1250$ K, $P' = 42$ kW/m, $D = 5.0283 \times 10^{-20}$ m²/s, and $t = 40,000$ h, and the burnup was approximately 12 GWd/tU. The radius was 10 μm for fission gas release. This situation is similar to the second case. The initial concentration of gas atoms is zero on the grain boundary and remains finite on the grain center. Gas atoms are not generated during LWR transient operation. The gas atoms begin to release when they reach grain boundaries. The release of gas atoms lasts for 40,000 h. Figure 8 indicates that the FGR fraction rises with increasing temperature. The results are slightly different between this model and Karahan's model, and the difference of results is within 15%.

Fission product gas release with microstructure dependence has been modeled for UO₂ fuel [51]. The main parameters were as follows: $T = 675$ K, $P' = 50$ kW/m for $D = 6.3283 \times 10^{-21}$ m²/s, $P' = 60$ kW/m for $D = 6.9323 \times 10^{-21}$ m²/s, $P' = 70$ kW/m for $D = 7.4877 \times 10^{-21}$ m²/s, and $t = 40,000$ h, and the burnup was approximately 30 MWd/kgU. There were three radiuses for fission gas release: 10 μm, 20 μm and 50 μm. This situation corresponds to the second case. The initial concentration of gas atoms is zero on the grain boundary and remains finite on the grain center. Gas atoms are not generated during LWR transient operation. The gas atoms begin to release when they reach the grain boundaries. The release of gas atoms lasts for 40,000 h. Figure 9 reflects that the FGR fraction drops with increasing linear heat generation rates, and the relationship is same as the above models between the FGR fraction and grain size. A small difference exists between this model and Bernard's model, but the greatest error was restricted within 5%, and thus, the results are convincing. Most of the error was within 5%, indicating that our model can provide reasonable results.

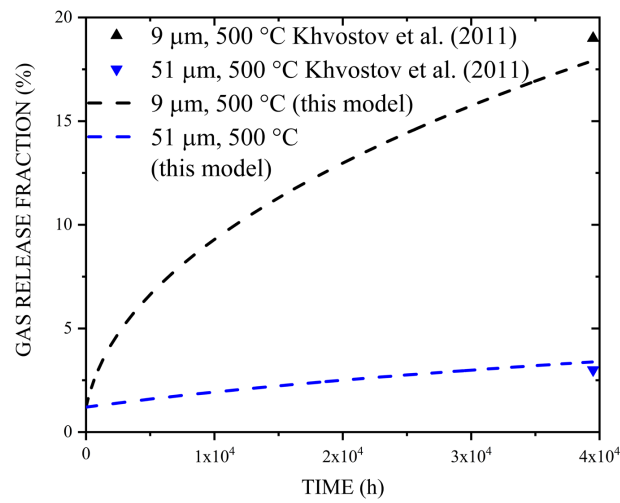


Figure 7. Gas release fraction versus time for constant gas production with different grain sizes in this model and Khvostov’s model [5].

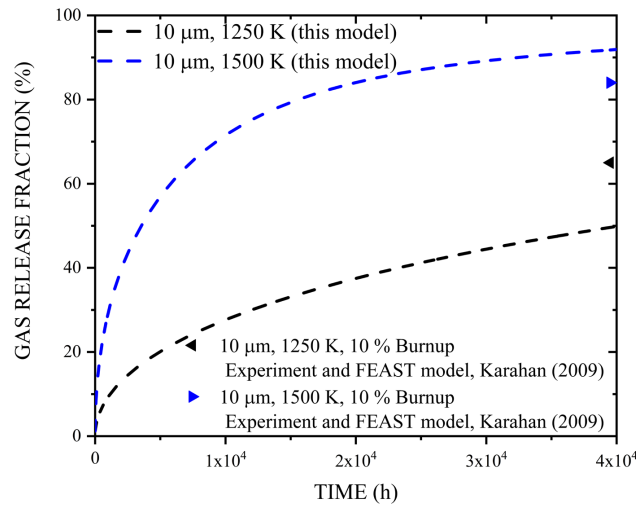


Figure 8. Gas release fraction versus time without gas production under different temperature conditions in this model, Karahan’s model, and experiments [50].

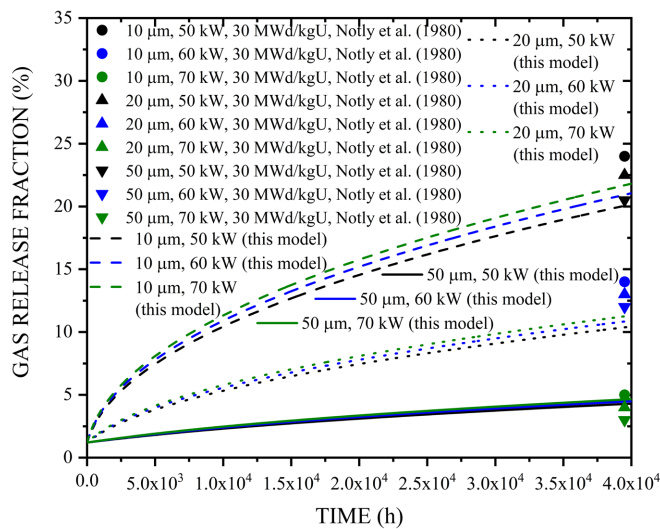


Figure 9. Gas release fraction versus time without gas production with different grain sizes and liner heat rates in this model and Notly’s model [51].

In order to investigate the sensitivity of fission gas release for diffusion coefficient, all parameters and conditions in Notly’s model were held constant except for the variation in the diffusion coefficient. Figure 10 demonstrates that the FGR fraction increases with a rising diffusion coefficient. The results of $a = 10 \mu\text{m}$, $P' = 70 \text{ kW/m}$ under one diffusion coefficient and 30 MWd/kgU , $a = 20 \mu\text{m}$, $P' = 60 \text{ kW/m}$ under half of diffusion coefficient and 30 MWd/kgU , and $a = 20 \mu\text{m}$ under all diffusion coefficients and liner heat rates in this model are close to Notly’s model. While some differences exist between this model and Notly’s model, the overall trend is consistent. Therefore, the outcomes are effective.

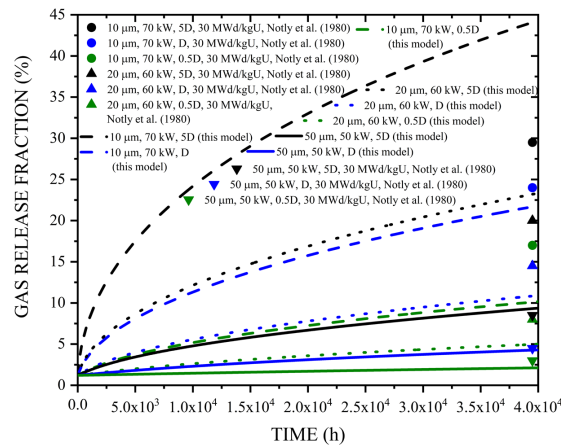


Figure 10. Gas release fraction versus time without gas production under different diffusion coefficients with unique grain sizes in this model and Notly’s model [51].

The isothermal fission gas release was modeled using the following parameters [3]: $T = 1300^\circ\text{C}$, $P' = 38 \text{ kW/m}$, $D = 1.6173 \times 10^{-18} \text{ m}^2/\text{s}$, and $t = 5 \text{ h}$, and the irradiation range was approximately 10 GWd/tUO_2 . There were three radiuses for fission gas release, $5 \mu\text{m}$, $7.5 \mu\text{m}$, and $11.5 \mu\text{m}$. The second case is applied in this situation. The initial concentration of gas atoms is zero on the grain boundary and remains finite in the grain center. Gas atoms are not generated during LWR transient operation. The gas atoms begin to release when they reach the grain boundaries. The release of gas atoms lasts for 3000 h. As shown in Figure 11, aside from the $5 \mu\text{m}$ case, the results in both of these two models are similar. The effect of grain size on the FGR fraction also corresponds to above models’ results.

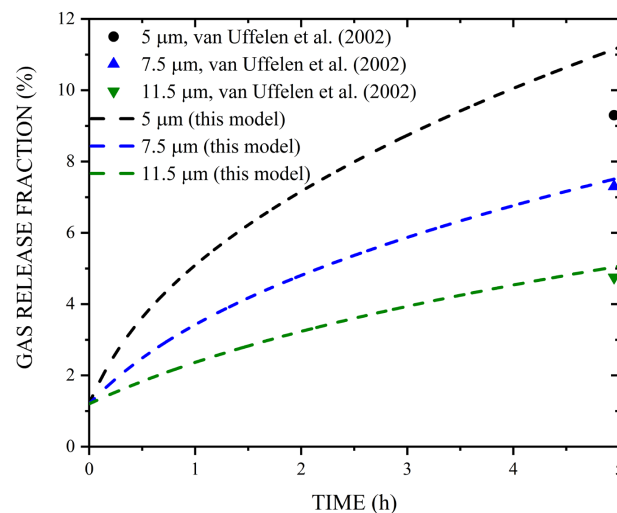


Figure 11. Gas release fraction versus time without constant gas production under different grain sizes in this model and van Uffelen’s model [3].

Fission gas release in oxide fuel was analyzed using BISON and TRANSURANUS with the following parameters [14]: $T = 1673$ K, $P' = 41.3$ kW/m, $D = 7.5595 \times 10^{-18}$ m²/s, $t = 10$ h, and the irradiation range was approximately 46 GWd/tU. The radius was 4.68 μ m. This condition suits in the second case. The initial concentration of gas atoms is zero on the grain boundary and remains finite on the grain center. Gas atoms are not generated during LWR transient operation. The gas atoms begin to release when they reach the grain boundaries. The release of gas atoms lasts for 80 h. As shown in Figure 12, the time in Barani's experiments is 80 h, but in this model, the time 10 h. The final values of the FGR fraction are close in these two models.

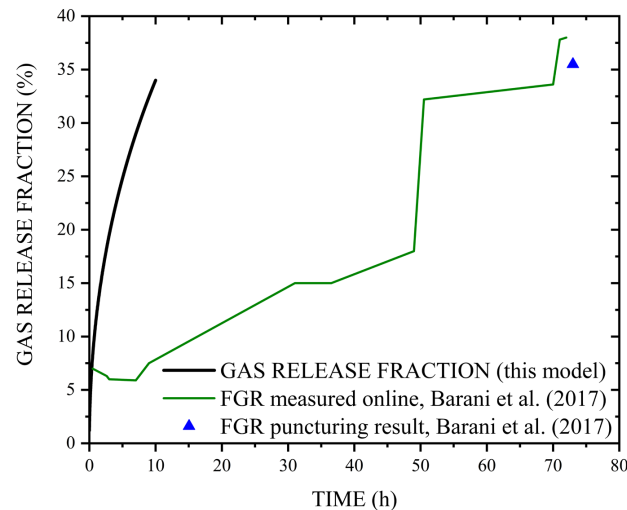


Figure 12. Gas release fraction versus time without gas production in this model and experimental measurements [14].

5. Conclusions

We presented an extended thermal activated fission gas release model for UO₂ fuel. The relevant physical phenomenon addressed in this model involves the diffusion of fission gases from the inner region of a UO₂ grain to the grain boundary. It focuses on the resolution between the grain and the grain boundary, as well as the accumulation and saturation of gas at the grain boundary. This study considers three cases under steady-state conditions: a perfect sink with gas production, a perfect sink without gas production, and an imperfect sink. A perfect sink with gas production is viewed as steady-state, and a perfect sink without gas production is regarded as a transient operation of a LWR. In particular, transient operation belongs to typical Class-II incidents in LWRs. In addition, the effect of FGR resolution on the grain boundary was also considered.

This model investigates how the fraction of fission gas release (FGR) varies over time, considering different factors such as the grain size, diffusion coefficient, temperature, and linear heat generation rate. Through the validation of the FGR model, several conclusions can be drawn. Gas atoms are released during transient operation faster than during steady-state operation, and the time of FGR is shorter than later in the model validation process when FGR fraction is equivalent. Fission gas will be released immediately during nuclear accidents. According to the results of the imperfect sink, it is evident that FGR is greatly influenced by resolution. The resolution will delay the onset time of FGR.

Furthermore, it was observed that the FGR fraction increases with higher diffusion coefficients and temperatures, while it decreases with larger grain sizes and higher linear heat generation rates. The diffusion coefficient, which is influenced by the temperature and linear heat generation rate, plays a significant role in driving the variation of the FGR fraction. Therefore, the impact of the diffusion coefficient on the FGR fraction is essentially a result of the effects of temperature and the linear heat generation rate. Importantly, all the results obtained in this model align with existing theories and conclusions. Hence, the

effectiveness of this model is deemed acceptable based on its consistency with established knowledge and findings.

Author Contributions: Conceptualization, J.G. and W.Z.; Methodology, S.C.; Investigation, K.W.; Data curation, J.G.; Writing—original draft, J.G. and W.Z.; Writing—review & editing, S.C. and K.W. All authors have read and agreed to the published version of the manuscript.

Funding: This work was supported by the Fundamental Research Funds for the Central Universities, Sun Yat-sen University (23qnpy75).

Conflicts of Interest: The authors declare no conflict of interest.

Abbreviations

Abbreviation

ATF	Accident-tolerant fuel
DOE-NE	Department of Energy's Nuclear Energy Office
FGR	Fission gas release
LOCA	Loss of coolant accident
LWR	Light water reactor
NPP	Nuclear power plant
PCMI	Pellet cladding mechanical interaction
PHWR	Pressurized heavy water reactor
PWR	Pressurized water reactor
RIA	Reactivity-initiated accident
VVER	Water–water power reactor

Nomenclature and units

a	Grain radius, m.
b	Probability of the intergranular atoms re-entering the solution, 1/s.
b'	Probability of atoms being resolved by fission spikes, 1/s.
B_1	Parameter of the incubation threshold calculation, MWd/tM.
B_2	Parameter of the incubation threshold calculation, K ⁻¹ .
B_3	Parameter of the incubation threshold calculation, K.
B_{MIN}	Parameter of the incubation threshold calculation, MWd/tM.
Bu	Burnup, MWd/tM.
c	Local concentration (number of gas atoms per unit volume), 1/m ³ .
c_0	Initial concentration (number of gas atoms per unit volume), 1/m ³ .
c_δ	Mean concentration at the grain boundaries, 1/m ³ .
D	Diffusion coefficient, m ² /s.
D_{01}	Ddiffusion coefficient constant, m ² /s.
D_{02}	Diffusion coefficient constant, m ² /s.
D_{03}	Diffusion coefficient constant, m ² /s.
D_{1+2+3}	Sum of intrinsic, thermal, and athermal diffusion coefficients, m ² /s.
D_1	Intrinsic diffusion coefficient, m ² /s.
D_2	Thermal diffusion coefficient, m ² /s.
D_3	Athermal diffusion coefficient, m ² /s.
$f(\theta)$	Geometry factor of the grain-edge bubble to the sphere.
F_0	Fission gas release fraction without resolution, %.
F_B	Fraction coverage of bubbles.
$F(t)$	Fission gas release fraction, %.
g	Probability of fission spikes trapping atoms within intragranular bubbles, 1/s. [27]
J	Flux exit of the grain, 1/(m ² ·s).
J_{rs}	Resolution flux, 1/(m ² ·s).
J_0	Flux without resolution, 1/(m ² ·s).
k	Boltzmann constant, 1.3806 × 10 ⁻²³ J/K.
L	Mean free-path between two bubbles, m.
n	Number of atoms in a bubble.
n_B	Bubble density, 1/m ² .

N	Density per unit area at the grain boundaries, $1/\text{m}^2$.
N_s	Threshold value of the surface density, $1/\text{m}^2$.
P	Bubble pressure, Pa.
P'	Linear heat generation rate (LHGR), kW/m .
P_{EXT}	Pressure, Pa.
R_B	Bubble radius, m.
t	Time, s.
t_i	Incubation time, s.
T	Temperature, K.
T_{01}	Parameter of the diffusion coefficient calculation, K.
T_{02}	Parameter of the diffusion coefficient calculation, K.
T_B	Parameter of the incubation threshold calculation, K.
T_{high}	High temperature for diffusion, K.
T_K	Local temperature, K.
T_{low}	Low temperature for diffusion, K.
V_B	Bubble volume, m^3 .
β	Creation rate, $1/(\text{m}^3 \cdot \text{s})$.
γ	Free surface energy, J/m^2 .
δ	Resolution depth, m.
θ	Semihedral angle.

References

- Burkes, D.E.; Casella, A.J.; Casella, A.M.; Luscher, W.G.; Rice, F.J.; Pool, K.N. Measurement of fission gas release from irradiated U-Mo monolithic fuel samples. *J. Nucl. Mater.* **2015**, *461*, 61–71. [[CrossRef](#)]
- Kim, H.C.; Cho, G. A hexagonal percolation model for zone-dependent pore interlinkage fraction of fission gas release. *Ann. Nucl. Energy* **1996**, *23*, 1445–1457. [[CrossRef](#)]
- Van Uffelen, P. *Modelling Isothermal Fission Gas Release*; IAEA: Vienna, Austria, 2002; Volume 333, pp. 17–31.
- Koo, Y.H.; Oh, J.Y.; Lee, B.H.; Tahk, Y.W.; Song, K.W. Artificial neural network modeling for fission gas release in LWR UO_2 fuel under RIA conditions. *J. Nucl. Mater.* **2010**, *405*, 33–43. [[CrossRef](#)]
- Khvostov, G.; Mikityuk, K.; Zimmermann, M.A. A model for fission gas release and gaseous swelling of the uranium dioxide fuel coupled with the FALCON code. *Nucl. Eng. Des.* **2011**, *241*, 2983–3007. [[CrossRef](#)]
- Zacharie, I.; Lansart, S.; Combette, P.; Trotabas, M.; Coster, M.; Groos, M. Thermal treatment of uranium oxide irradiated in pressurized water reactor: Swelling and release of fission gases. *J. Nucl. Mater.* **1998**, *255*, 85–91. [[CrossRef](#)]
- Viswanathan, U.K.; Sah, D.N.; Rath, B.N.; Anantharaman, S. Measurement of fission gas release, internal pressure and cladding creep rate in the fuel pins of PHWR bundle of normal discharge burnup. *J. Nucl. Mater.* **2009**, *392*, 545–551. [[CrossRef](#)]
- Rahmani, Y. Feasibility study of chabazite absorber tube utilization in online absorption of released gaseous fission products and substitution of burnable absorber rods with chabazite absorber tubes in VVER-1000 reactor series. *Ann. Nucl. Energy* **2017**, *102*, 56–76. [[CrossRef](#)]
- Terrani, K.A. Accident tolerant fuel cladding development: Promise, status, and challenges. *J. Nucl. Mater.* **2018**, *501*, 13–30.
- Alrwashdeh, M.; Alameri, S.A. Chromium-coated zirconium cladding neutronics impact for APR-1400 reactor core. *Energies* **2022**, *15*, 8008. [[CrossRef](#)]
- Barani, T.; Pastore, G.; Pizzocri, D.; Andersson, D.A.; Matthews, C.; Alfonsi, A.; Gamble, K.A.; van Uffelen, P.; Luzzi, L.; Hales, J.D. Multiscale modeling of fission gas behavior in U_3Si_2 under LWR conditions. *J. Nucl. Mater.* **2019**, *522*, 97–110. [[CrossRef](#)]
- Rest, J.; Cooper, M.W.D.; Spino, J.; Turnbull, J.A.; van Uffelen, P.; Walker, C.T. Fission gas release from UO_2 nuclear fuel: A review. *J. Nucl. Mater.* **2019**, *513*, 310–345. [[CrossRef](#)]
- Barani, T.; Pastore, G.; Magni, A.; Pizzocri, D.; Van Uffelen, P.; Luzzi, L. Modeling intra-granular fission gas bubble evolution and coarsening in uranium dioxide during in-pile transients. *J. Nucl. Mater.* **2020**, *538*, 152195. [[CrossRef](#)]
- Barani, T.; Bruschi, E.; Pizzocri, D.; Pastore, G.; van Uffelen, P.; Williamson, R.L.; Luzzi, L. Analysis of transient fission gas behaviour in oxide fuel using BISON and TRANSURANUS. *J. Nucl. Mater.* **2017**, *486*, 96–110. [[CrossRef](#)]
- Liu, R.; Zhou, W.; Prudil, A.; Chan, P.K. Multiphysics modeling of UO_2 -SiC composite fuel performance with enhanced thermal and mechanical properties. *Appl. Therm. Eng.* **2016**, *107*, 86–100. [[CrossRef](#)]
- Tonks, M.; Andersson, D.; Devanathan, R.; Dubourg, R.; El-Azab, A.; Freyss, M.; Iglesias, F.; Kulacsy, K.; Pastore, G.; Phillpot, S.R.; et al. Unit mechanisms of fission gas release: Current understanding and future needs. *J. Nucl. Mater.* **2018**, *504*, 300–317. [[CrossRef](#)]
- Guo, J.; Lai, H.; Zhou, W.; Wei, J. Fission gas behaviors and relevant phenomena in different nuclear fuels: A review of models and experiments. *Front. Energy Res.* **2022**, *10*, 39. [[CrossRef](#)]
- Dowling, D.M.; White, R.J.; Tucker, M.O. The Effect of Irradiation-Induced Re-Resolution on Fission Gas Release. *J. Nucl. Mater.* **1982**, *110*, 37–46. [[CrossRef](#)]

19. Elton, P.T.; Lassmann, K. Calculational Methods for Diffusional Gas Release. *Nucl. Eng. Des.* **1985**, *101*, 259–265. [[CrossRef](#)]
20. Forsberg, K.; Massih, A.R. Fission Gas Release under Time-Varying Conditions. *J. Nucl. Mater.* **1985**, *127*, 141–145. [[CrossRef](#)]
21. Forsberg, K.; Massih, A.R. Diffusion Theory of Fission Gas Migration in Irradiated Nuclear Fuel UO₂. *J. Nucl. Mater.* **1985**, *135*, 140–148. [[CrossRef](#)]
22. Hargreaves, R.; Collins, D.A.; Brit, J. Quantitative model for fission gas release and swelling in irradiated uranium dioxide. *Nucl. Energy Soc.* **1976**, *15*, 311.
23. Ito, K.; Iwasaki, R.; Iwano, Y. Finite Element Model for Analysis of Fission Gas Release from UO₂ Fuel. *J. Nucl. Sci. Technol.* **1985**, *22*, 129–138. [[CrossRef](#)]
24. Speight, M.V. A Calculation on the Migration of Fission Gas in Material Exhibiting Precipitation and Re-solution of Gas Atoms Under Irradiation. *Nucl. Sci. Eng.* **1969**, *37*, 180–185. [[CrossRef](#)]
25. Turnbull, J.A. The Effect of Grain Size on the Swelling and Gas Release Properties of UO₂ During Irradiation. *J. Nucl. Mater.* **1974**, *50*, 62–68. [[CrossRef](#)]
26. White, R.J.; Tucker, M.O. A New Fission-Gas Release Model. *J. Nucl. Mater.* **1983**, *118*, 1–38. [[CrossRef](#)]
27. Olander, D.R. *Fundamental Aspects of Nuclear Reactor Fuel Elements*; ERDA; University of California: Berkeley, CA, USA, 1974.
28. Vitanza, C.; Kolstad, E.; Graziani, U. Fission Gas Release from UO₂ Pellet Fuel at High Burn-up. In Proceedings of the ANS Topical Meeting on LWR Fuel Performance, Portland, WA, USA, 29 April–2 May 1979; p. 361.
29. Booth, A.H. *A Method of Calculating Fission Gas Diffusion from UO₂ Fuel and Its Application to the X-2-f Loop Test*; Rapport Atomic Energy of Canada Limited CRDC-721; IAEA: Toronto, ON, Canada, 1957. Available online: <https://www.osti.gov/biblio/4331839> (accessed on 29 August 2023).
30. Turnbull, J.A.; Friskney, C.A.; Findlay, J.R.; Johnson, F.A.; Water, A.J. The Diffusion Coefficients of Gaseous and Volatile Species during the Irradiation of Uranium Dioxide. *J. Nucl. Mater.* **1982**, *107*, 168–184. [[CrossRef](#)]
31. Turnbull, J.A.; White, R.J.; Wise, C. The Diffusion Coefficient for Fission Gas Atoms in Uranium Dioxide. In *Meeting on Water Reactor Fuel Element Computer Modelling in Steady State, Transient and Accident Conditions*; IAEA Technology Company: Preston, UK, 1988.
32. Matzke, H. Gas release mechanisms in UO₂—A critical review. *Radiat. Eff.* **1980**, *53*, 219–242. [[CrossRef](#)]
33. Combette, P.; Zacharie, I. Reply to the comments by J.H. Evans about two papers ‘Thermal treatment of UO₂ irradiated in a pressurized water reactor: Swelling and release of fission gases’ and ‘Microstructural analysis and modelling of intergranular swelling of an irradiated UO₂ fuel treated at high temperature’ by I. Zacharie, S. Lansart, P. Combette, M. Trotabas, M. Coster and M. Groos. *J. Nucl. Mater.* **1999**, *275*, 112–114.
34. Kogai, T. Modelling of fission gas release and gaseous swelling of light water reactor fuels. *J. Nucl. Mater.* **1997**, *244*, 131–140. [[CrossRef](#)]
35. Baker, C. The fission gas bubble distribution in uranium dioxide from high temperature irradiated SGHWR fuel pins. *J. Nucl. Mater.* **1977**, *66*, 283–291. [[CrossRef](#)]
36. Cornell, R.M. The growth of fission gas bubbles in irradiated uranium dioxide. *Philos. Mag.* **1969**, *19*, 539–554. [[CrossRef](#)]
37. Davis, D.; Long, G. AERE Rep. No. 4347. In *Technical Report*; Atomic Energy Research Establishment: Harwell, UK, 1963.
38. Miekeley, W.; Felix, F.W. Effect of stoichiometry on diffusion of xenon in UO₂. *J. Nucl. Mater.* **1972**, *42*, 297–306. [[CrossRef](#)]
39. Ronchi, C. Thermophysical properties affecting safety and performance of nuclear fuel. *High Temp.* **2007**, *45*, 552–571. [[CrossRef](#)]
40. Walker, C.T.; Lassmann, K. Fission gas and caesium gradients in single grains of transient tested UO₂ Fuel: Results of an EPMA investigation. *J. Nucl. Mater.* **1986**, *138*, 155–161. [[CrossRef](#)]
41. Klipfel, M.; Di Marcello, V.; Schubert, A.; van de Laar, J.; van Uffelen, P. Towards a multiscale approach for assessing fission product behaviour in UN. *J. Nucl. Mater.* **2013**, *442*, 253–261. [[CrossRef](#)]
42. Sato, I.; Katsuyama, K.; Arai, Y. Fission gases and helium gas behavior in irradiated mixed oxide fuel pin. *J. Nucl. Mater.* **2011**, *416*, 151–157. [[CrossRef](#)]
43. Thetford, R.; Mignanelli, M. The chemistry and physics of modelling nitride fuels for transmutation. *J. Nucl. Mater.* **2003**, *320*, 44–53. [[CrossRef](#)]
44. Bernard, L.C.; Bonnaud, E. Finite volume method for fission gas release modeling. *J. Nucl. Mater.* **1997**, *244*, 75–84. [[CrossRef](#)]
45. Bernaudat, C. Mechanical behaviour modelling of fractured nuclear fuel pellets. *Nucl. Eng. Des.* **1995**, *156*, 373–381. [[CrossRef](#)]
46. Walker, C.T.; Knappik, P.; Mogensen, M. Concerning the Development of Grain Face Bubbles and Fission Gas Release in UO₂ Fuel. *J. Nucl. Mater.* **1988**, *160*, 10–23. [[CrossRef](#)]
47. Zimmermann, H. Investigations on Swelling and Fission Gas Behaviour in Uranium Dioxide. *J. Nucl. Mater.* **1978**, *75*, 154–161. [[CrossRef](#)]
48. Brearly, I.R.; MacInnes, D.A. An Improved Equation of State for Inert Gases at High Pressures. *J. Nucl. Mater.* **1980**, *95*, 239–252. [[CrossRef](#)]
49. Lee, C.B.; Yong, S.Y.; Dae, H.K.; Sun, K.K.; Je, G.B. A New Mechanistic and Engineering Fission Gas Release Model for a Uranium Dioxide Fuel. *J. Nucl. Sci. Technol.* **2008**, *45*, 60–71. [[CrossRef](#)]

50. Karahan, A. Modeling of Thermo-Mechanical and Irradiation Behavior of Metallic and Oxide Fuels for Sodium Fast Reactor. Ph.D. Thesis, MIT, Cambridge, MA, USA, 2009.
51. Notley, M.J.F.; Hastings, I.J. A microstructure-dependent model for fission product gas release and swelling in UO₂ fuel. *Nucl. Eng. Des.* **1980**, *56*, 163–175. [[CrossRef](#)]

Disclaimer/Publisher's Note: The statements, opinions and data contained in all publications are solely those of the individual author(s) and contributor(s) and not of MDPI and/or the editor(s). MDPI and/or the editor(s) disclaim responsibility for any injury to people or property resulting from any ideas, methods, instructions or products referred to in the content.